



Published in final edited form as:

Nanoscale. 2016 January 28; 8(4): 2116–2122. doi:10.1039/c5nr07552a.

Dual-enhanced photothermal conversion properties of reduced graphene oxide-coated gold superparticles for light-triggered acoustic and thermal theranostics[†]

Li-Sen Lin^{a,b}, Xiangyu Yang^b, Gang Niu^b, Jibin Song^b, Huang-Hao Yang^a, and Xiaoyuan Chen^b

^aThe Key Lab of Analysis and Detection Technology for Food Safety of the MOE, College of Chemistry, Fuzhou University, Fuzhou 350108, China

^bLaboratory of Molecular Imaging and Nanomedicine (LOMIN), National Institute of Biomedical Imaging and Bioengineering (NIBIB), National Institutes of Health (NIH), Bethesda, Maryland 20892, USA

Abstract

A rational design of highly efficient photothermal agents that possess excellent light-to-heat conversion properties is a fascinating topic in nanotheranostics. Herein, we present a facile route to fabricate size-tunable reduced graphene oxide (rGO)-coated gold superparticles (rGO-GSPs) and demonstrate their dual-enhanced photothermal conversion properties for photoacoustic imaging and photothermal therapy. For the first time, graphene oxide (GO) was directly used as an emulsifying agent for the preparation of gold superparticles (GSPs) with near-infrared absorption by the emulsion method. Moreover, GO spontaneously deposited on the surface of GSPs could also act as the precursor of the rGO shell. Importantly, both the plasmonic coupling of the self-assembled gold nanoparticles and the interaction between GSPs and rGO endow rGO-GSPs with enhanced photothermal conversion properties, allowing rGO-GSPs to be used for sensitive photoacoustic detection and efficient photothermal ablation of tumours *in vivo*. This study provides a facile approach to prepare colloidal superparticles–graphene hybrid nanostructures and will pave the way toward the design and optimization of photothermal nanomaterials with improved properties for theranostic applications.

1. Introduction

Theranostics, the combination of diagnostic and therapeutic capabilities within a single platform, provides great opportunities in the fight against various diseases.^{1–5} In particular, light-triggered theranostics has attracted tremendous attention over the past few years because of its excellent spatiotemporal controllability for disease treatment, as well as the advantages of optical imaging including noninvasive, nonionizing radiation and high spatial resolution.^{6–9} Moreover, the use of near-infrared (NIR) light with superior tissue penetration ability greatly promotes the development of light-triggered theranostics including

[†]Electronic supplementary information (ESI) available. See DOI: 10.1039/c5nr07552a

Correspondence to: Jibin Song; Huang-Hao Yang; Xiaoyuan Chen.

photoacoustic imaging (PAI) and photothermal therapy (PTT).^{10–12} Recently, NIR photothermal agents (PTAs) that can generate heat to induce the formation of an acoustic wave and cell death upon appropriate light irradiation have been successfully utilized for simultaneous PAI and PTT.^{13–15} Importantly, the photothermal conversion ability of PTAs is one of the most important factors for achieving highly sensitive PAI and effective PTT.^{16,17} Therefore, the development of PTAs with excellent photothermal conversion properties is highly desired for cancer diagnosis and therapy.

With recent developments in nanotechnology, plasmonic metal nanoparticles have been successfully employed as PTAs due to their localized surface plasmon resonance (LSPR).^{18–21} It is well known that the LSPR absorption of plasmonic nanoparticles arising from the collective oscillation of conduction electrons can be tuned by controlling the size, shape, dielectric environment, and interparticle distance.^{22–25} Especially, the assembly of gold nanoparticles (GNPs) can not only lead to the red-shift of the LSPR peak to the NIR region by decreasing the interparticle distance but also enhance the photothermal conversion properties, which is attributed to the strong plasmonic coupling effect between adjacent GNPs.²⁶ Interestingly, several studies have shown that the combination of plasmonic nanostructures and carbon-based materials (CBM) is an effective approach to achieve improvement in optical properties.^{27–33} For example, GNPs have been integrated with graphene to greatly enhance the photocurrent and surface enhanced Raman scattering performances.^{27,33} Nevertheless, to the best of our knowledge, there is no study on the fabrication of gold assemblies–CBM nanocomposites and the assessment of their photothermal conversion properties for theranostic applications.

Herein, we report the facile synthesis of size-tunable reduced graphene oxide (rGO)-coated gold superparticles (rGO-GSPs) through an emulsion-based self-assembly method without using any additional surfactants as emulsifying agents and their dual-enhanced photothermal conversion properties for light-triggered acoustic and thermal theranostics (Scheme 1). Since an emulsifying agent is one of the most important components for preparing an oil-in-water (O/W) emulsion system, some amphiphilic surfactants have been used in the construction of colloidal superparticles.³⁴ In this study, for the first time, graphene oxide (GO) with amphiphilic properties resulting from the presence of hydrophilic edges and a more hydrophobic basal plane was directly employed as the emulsifying agent to produce the O/W emulsion system for the preparation of gold superparticles (GSPs). After emulsification by ultrasonic treatment and evaporation of chloroform from the emulsion droplets, hydrophobic GNPs could self-assemble into dense GSPs, which possess strong NIR absorption and enhanced photothermal conversion performance due to the plasmonic coupling of adjacent GNPs.²⁶ Meanwhile, GO could be spontaneously deposited on the surface of GSPs, leading to the successful formation of GO-coated gold super-particles (GO-GSPs). Moreover, the size of GO-GSPs could be tuned by simply varying the concentration of GNPs in the oil phase. Impressively, after the reduction of the GO shell, the obtained rGO-GSPs exhibited remarkable enhancement in the photothermal effect compared to the simple mixture of GSPs and rGO, which can be attributed to the interaction between GSPs and rGO.³² After modifying rGO-GSPs with 1,2-distearoyl-phosphatidylethanolamine-methyl-polyethyleneglycol (DSPE-mPEG, $M_w = 5000$) through hydrophobic interactions,

PEGylated rGO-GSPs (PEG-rGO-GSPs) with excellent photo-stability and biocompatibility showed great promise as superior PTAs for *in vivo* simultaneous PAI and PTT.

2. Experimental section

2.1 Materials

Gold(III) chloride hydrate, 1-octadecene (ODE, 90%), oleylamine (OAm, 70%), oleic acid (OA, 90%), hydrazine monohydrate ($\text{NH}_2\text{NH}_2\cdot\text{H}_2\text{O}$), hexadecyltrimethylammonium bromide (CTAB, 99%), sodium borohydride (NaBH_4 , 99%), L-ascorbic acid (AA, 99%), silver nitrate (AgNO_3 , 99%) and 3-(4,5-dimethyl-thiazol-2-yl)-2,5-diphenyltetrazolium bromide (MTT) were purchased from Sigma-Aldrich (St. Louis, MO, USA). All chemicals were used without further purification, and Milli-Q water was used throughout the study.

2.2 Synthesis of hydrophobic GNPs

Hydrophobic GNPs were prepared according to the previously reported method.³⁵ Briefly, ODE (60 mL), OAm (4.5 mL) and OA (4.5 mL) were mixed together in a flask and the solution was heated at 120 °C for 30 min under an argon atmosphere. Then, a solution containing gold(III) chloride hydrate (120 mg), ODE (15 mL) and OAm (2 mL) was injected into the flask. After heating up to 150 °C for 30 min, the resulting GNPs were precipitated by adding isopropanol, collected by centrifugation, and then dispersed in chloroform.

2.3 Synthesis of GO

GO was synthesized by a modified Hummers method.³⁶ Graphite (1 g) and NaNO_3 (1 g) were dissolved in concentrated H_2SO_4 (46 mL). After the slow addition of KMnO_4 (6 g), the mixture was stirred for 72 h. Then, water (40 mL) was added and the temperature was further increased to 90 °C. After further diluting with water (200 mL), the mixture was incubated for another 72 h before the addition of H_2O_2 (30%, 6 mL). Subsequently, the mixture was washed with 4% HCl and distilled water. The obtained graphite oxide was mixed with water and ultrasonicated for 4 h. Finally, the resulting GO solution was centrifuged at 12 000 rpm for 15 min and the supernatant was collected for further use.

2.4 Synthesis of rGO-GSPs

In a typical synthesis of GO-GSPs with a diameter of ~90 nm, a chloroform solution of hydrophobic GNPs (1.0 mL, 10 mg mL⁻¹) was added to aqueous GO solution (10 mL, 0.1 mg mL⁻¹). After emulsification by ultrasonic treatment, the mixture was heated at 60 °C under constant stirring for 30 min to remove chloroform. Then, GO-GSPs were obtained by centrifugation and washed with water several times. The GO-GSPs with diameters of ~60 nm and ~130 nm were prepared by changing the concentration of GNPs in chloroform to 5 mg mL⁻¹ and 20 mg mL⁻¹, respectively. In order to reduce the GO shell, 10 μL of $\text{NH}_2\text{NH}_2\cdot\text{H}_2\text{O}$ was added to 10 mL of aqueous GO-GSP solution (1 mg mL⁻¹) and the mixture was heated at 90 °C for 1 h, the obtained rGO-GSPs were collected by centrifugation and washed with water. For further PEGylation, rGO-GSPs were dispersed into aqueous DSPE-mPEG ($M_w = 5000$) solution (10 mL, 1 mg mL⁻¹). After ultrasonic treatment for 2 h, PEGylated rGO-GSPs were washed with water to remove excess DSPE-mPEG.

2.5 Synthesis of GSPs

A solution containing hydrophobic GNPs (10 mg) in chloroform (1 mL) was added to the aqueous solution of Pluronic F127 (10 mL, 0.01 mg mL⁻¹) and the mixture was emulsified by ultrasonication for 5 min. After the evaporation of chloroform at 60 °C, GSPs were collected and washed with water by centrifugation.

2.6 Synthesis of rGO-coated gold nanorods (rGO-GNRs)

Gold nanorods (GNRs) were prepared by the seed-mediated growth method.³⁷ Briefly, CTAB solution (5 mL, 0.2 M) was mixed with HAuCl₄ (5 mL, 0.5 mM). After the addition of NaBH₄ solution (0.6 mL, 0.01 M) under vigorous stirring, the seeds were formed immediately. The growth solution contained CTAB (50 mL, 0.2 M), HAuCl₄ (50 mL, 1 mM), AgNO₃ (1.1 mL, 10 mM) and AA (0.7 mL, 0.0788 M). Growth was initiated by adding 0.12 mL seeds and the temperature of the growth solution was maintained at 27–30 °C. Then, the CTAB-coated GNRs were modified with GO through an electrostatic interaction. A solution of GNRs was dropwise added to the GO solution and the mixture was stirred overnight. After the removal of excess GO by centrifugation, the GO-coated GNRs were reduced by NH₂NH₂·H₂O at 90 °C for 1 h.

2.7 Assessment of photothermal conversion and photoacoustic (PA) properties

To compare photothermal conversion properties, aqueous dispersions of different gold-based nanomaterials with the same optical density at 808 nm (OD₈₀₈) of 1.0 were irradiated by an NIR laser (808 nm, 1 W cm⁻²) for 5 min. The temperatures of the solutions were measured by an infrared thermal camera. To further assess the photothermal effect of rGO-GSPs, aqueous rGO-GSP solutions (OD₈₀₈ = 1.0) were irradiated by the 808 nm laser at different power densities (0.2–1.0 W cm⁻²) for 5 min.

To investigate the PA performance, different gold-based nanomaterials were dispersed in water at certain OD₈₀₈, and then PA images were obtained using a Vevo 2100 LAZR system (VisualSonics Inc., New York, NY) equipped with a 40 MHz, 256-element linear array transducer.

2.8 *In vitro* PTT

U87MG cells were incubated with or without PEG-rGO-GSPs (100 µg mL⁻¹) for 4 h and then exposed to an 808 nm laser at different power densities (0.3 and 0.8 W cm⁻²) for 5 min. After co-staining with calcein AM and propidium iodide (PI) for 30 min, the cells were imaged by an Olympus IX81 fluorescence microscope to capture the green fluorescence of live cells and the red fluorescence of dead cells.

To quantitatively evaluate the photothermal cytotoxicity of PEG-rGO-GSPs, U87MG cells seeded in 96-well plates were incubated with or without PEG-rGO-GSPs (100 µg mL⁻¹) for 4 h. After exposure to the NIR laser at different power densities (0.3 and 0.8 W cm⁻²) for 5 min, the cells were incubated for another 24 h. Then, the standard MTT assay was carried out to determine the cell viability.

2.9 Tumour model

All animal experiments were performed according to a protocol approved by the National Institutes of Health Clinical Center Animal Care and Use Committee (NIH CC/ACUC). Female nude mice were subcutaneously implanted with 1×10^6 U87MG cells in the front flank. The *in vivo* studies were started when the tumour volumes reached about 60 mm^3 .

2.10 *In vivo* PAI

200 μL of PEG-rGO-GSPs (1 mg mL^{-1}) or PBS was intravenously injected into the tail vein of U87MG tumour-bearing mice. Then, the PA images of mice were obtained using the PA system at different time points.

2.11 *In vivo* PTT

The U87MG tumour-bearing mice were injected intravenously with 200 μL of PEG-rGO-GSPs (1 mg mL^{-1}) or PBS. At 24 h post-injection, mice were exposed to an 808 nm laser at different power densities (0.3 and 0.8 W cm^{-2}) for 5 min. Real-time thermal imaging was carried out using the infrared thermal camera.

The photothermal therapeutic efficacy of PEG-rGO-GSPs was investigated by measuring the volumes of the tumours after different treatments. The U87MG tumour-bearing mice were randomly divided into four groups ($n = 5$ for each group). For the photothermal therapy group, mice were intravenously injected with PEG-rGO-GSPs ($200 \mu\text{L}$, 1 mg mL^{-1}) and then irradiated by an NIR laser (0.8 W cm^{-2} , 5 min) at 24 h post-injection. For other groups, mice were treated with PBS before laser irradiation or PEG-rGO-GSPs only. The tumour sizes were measured by a caliper and calculated as volume = (tumour length) \times (tumour width)²/2.

3. Results and discussion

3.1 Preparation and characterization of rGO-GSPs

In the typical synthesis of GO-GSPs, a chloroform solution of oleylamine/oleic acid-capped GNPs with diameter of about 14 nm (Fig. 1a) was added into an aqueous solution of GO with an average lateral size of about 150 nm (Fig. 1b). After ultrasonic treatment, the obtained O/W emulsion was kept at $60 \text{ }^\circ\text{C}$ for 30 min to allow the evaporation of chloroform and the subsequent formation of the GO-GSPs, which was accompanied by a colour change from red to blue (Fig. S1[†]). As shown in the transmission electron microscopy (TEM) images (Fig. 1c), differently sized (60 nm, 90 nm and 130 nm) GO-GSPs could be obtained by changing the concentration of GNPs in chloroform. In addition, GO-GSPs showed a red-shift in LSPR as compared to individual GNPs (Fig. 1d). Moreover, the red-shift of the LSPR peak increased with the size of GO-GSPs. It has been reported that nanoparticles in the size range of 10–100 nm are accumulated preferentially at the tumour sites through the enhanced permeability and retention (EPR) effect.³⁸ Thus, 90 nm GO-GSPs with strong NIR absorption were used in the following studies. In order to reduce the GO shell, GO-GSPs were mixed with hydrazine hydrate and heated at $90 \text{ }^\circ\text{C}$ for 1 h. The absorption peak of the

[†]Electronic supplementary information (ESI) available. See DOI: 10.1039/c5nr07552a

GO shell at 230 nm shifted to 270 nm after the treatment (Fig. S2[†]), suggesting that GO was effectively reduced to rGO by hydrazine. In addition, the increase of the D/G band ratio in Raman spectra further demonstrated the successful reduction of the GO shell (Fig. S3[†]). Furthermore, there was no obvious change in the morphology of the GO-GSPs during the reduction process (Fig. 1e).

3.2 Photothermal conversion and PA properties

To evaluate the potential of rGO-GSPs as PTAs, we first investigated their photothermal conversion properties. The aqueous dispersions of different gold-based nanomaterials with the same OD₈₀₈ of 1.0 were irradiated by an 808 nm laser with a power density of 1 W cm⁻² for 5 min. It can be seen in Fig. 2a that rGO-GSPs, rGO-GNRs (Fig. S4[†]), the mixture of GSPs (Fig. S5[†]) and rGO, GO-GSPs, GSPs, and GNRs increased the temperature by 49.3, 38.7, 36.0, 35.3, 34.3, and 25.1 °C, respectively. Significantly enhanced photothermal conversion was observed in GSPs compared to GNRs and rGO-GSPs compared to the mixture of GSPs and rGO, which could be attributed to the strong plasmonic coupling of self-assembled GNPs and the interaction of GSPs with rGO, respectively.^{26,32} Moreover, rGO-GSPs showed the laser-power-dependent photothermal effect (Fig. 2b and c) and excellent photostability without an apparent morphology change even after 30 min irradiation at 1.0 W cm⁻² (Fig. S6[†]). Since the photothermal effect can give rise to thermoelastic expansion and the subsequent generation of acoustic wave, the PA performance of rGO-GSPs was then studied. As shown in Fig. 2d and e, rGO-GSPs provided a significantly higher PA signal compared to the mixture of GSPs and rGO upon NIR irradiation, which is consistent with their photothermal effect. These results demonstrated that rGO-GSPs with dual-enhanced photothermal conversion properties can efficiently generate heat and an acoustic signal upon NIR irradiation.

3.3 *In vitro* PTT

It has been reported that cancer cells can be killed by heating at 42 °C for 15–60 min, and the duration can be shortened to 4–6 min when the temperature is raised to over 50 °C.³⁹ The strong photothermal effect of rGO-GSPs prompted us to investigate their ability to kill cancer cells upon NIR irradiation. In addition, PEGylated rGO-GSPs exhibit excellent stability in different media (Fig. S7[†]). U87MG human glioma cells were incubated with 100 µg mL⁻¹ of PEG-rGO-GSPs for 4 h and then irradiated by an 808 nm laser at different power densities for 5 min. After co-staining with calcein AM and PI, cells were observed using a fluorescence microscope to capture the green fluorescence of calcein AM and the red fluorescence of PI. It can be seen in Fig. 3a that PEG-rGO-GSPs could effectively kill the cancer cells under NIR irradiation at a power density of 0.8 W cm⁻², while neither the laser irradiation nor the PEG-rGO-GSPs alone could result in cell death. In addition, the photothermal cytotoxicity of PEG-rGO-GSPs was further quantitatively assessed using a standard MTT assay. As shown in Fig. 3b, the viability of U87MG cells treated with PEG-rGO-GSPs and NIR laser significantly decreased with increasing power density. In comparison, no apparent cytotoxicity was observed after the cells were incubated with PEG-rGO-GSPs even at a high concentration of 200 µg mL⁻¹ for 24 h (Fig. 3c), indicating the low cytotoxicity of the PEG-rGO-GSPs. The above results suggested that the highly

biocompatible PEG-rGO-GSPs could effectively induce cell death through the NIR light-induced photothermal effect.

3.4 *In vivo* PAI

PAI, a hybrid imaging technique that provides strong optical absorption contrast and high ultrasonic resolution, has received increasing attention in cancer diagnosis.^{40,41} Considering that rGO-GSPs can efficiently convert NIR light into an acoustic signal, we evaluated their feasibility as PA agents for *in vivo* PAI. U87MG tumour-bearing mice were intravenously injected with PEG-rGO-GSPs (200 μL , 1 mg mL^{-1}) and imaged using a PAI system with an 800 nm laser as the excitation source. As shown in Fig. 4, the PA signal in tumour tissue was greatly enhanced after 24 h of injection with PEG-rGO-GSPs, indicating the efficient accumulation of PEG-rGO-GSPs in the tumour, which could be attributed to the EPR effect. These results confirmed the great potential of PEG-rGO-GSPs for *in vivo* PAI, which could be further used to guide the NIR laser irradiation in PTT and consequently enhance the therapeutic efficacy and minimize the damage to the surrounding tissues.

3.5 *In vivo* PTT

Encouraged by the *in vitro* PTT efficacy of PEG-rGO-GSPs, we then examined the possibility of using PEG-rGO-GSPs for *in vivo* PTT. First, photothermal imaging was used to verify the temperature change of tumour-bearing mice exposed to laser irradiation at 24 h post-intravenous injection of PEG-rGO-GSPs (200 μL , 1 mg mL^{-1}). As shown in Fig. 5a, the surface temperature of the tumour rapidly increased from $\sim 30\text{ }^{\circ}\text{C}$ to $\sim 58\text{ }^{\circ}\text{C}$ within 5 min of 808 nm laser irradiation at a power density of 0.8 W cm^{-2} . In contrast, the temperature of the tumour in the mouse intravenously injected with PBS increased by only $\sim 4\text{ }^{\circ}\text{C}$ under the same laser irradiation conditions. To further verify the photothermal therapeutic effect of PEG-rGO-GSPs, the U87MG tumour-bearing mice were randomly divided into four groups ($n = 5$ for each group): (1) control group without any treatment, (2) intravenous injection with PBS + laser irradiation (0.8 W cm^{-2} , 5 min), (3) intravenous injection with PEG-rGO-GSPs only (200 μL , 1 mg mL^{-1}), and (4) intravenous injection with PEG-rGO-GSPs (200 μL , 1 mg mL^{-1}) + laser irradiation (0.8 W cm^{-2} , 5 min). It can be seen in Fig. 5b–d that tumours in mice intravenously injected with PEG-rGO-GSPs for 24 h were successfully eliminated without reoccurrence after NIR laser irradiation. However, tumours in the control, PBS + laser irradiation, and PEG-rGO-GSPs only groups showed relatively rapid growth. Moreover, mice treated with PEG-rGO-GSPs and laser irradiation survived over 40 days, while mice in the other three groups showed average life spans of not more than 20 days. Moreover, hematoxylin and eosin (H&E)-stained tumour sections collected immediately after laser irradiation showed that the tumour cells after PTT in group 4 were severely destroyed, while no detectable damage was observed in the other three groups (Fig. 5e). In addition, neither obvious body weight drop nor noticeable organ damage was observed after PTT treatment (Fig. S8–9[†]), indicating the good biocompatibility of PEG-rGO-GSPs *in vivo*. These results suggested that PEG-rGO-GSPs could act as promising PTAs for *in vivo* PTT of cancer.

4. Conclusions

In summary, we have developed a novel theranostic nanoplat-form based on reduced graphene oxide-coated gold superparticles (rGO-GSPs) with dual-enhanced photothermal conversion properties for *in vivo* photoacoustic imaging (PAI) and photo-thermal therapy (PTT) of cancer. By using an emulsion-based self-assembly method that directly utilizes graphene oxide (GO) as a surfactant to form an oil-in-water emulsion system, the preparation of gold superparticles (GSPs) accompanied by the coating of their surface with GO was successfully achieved for the first time. In addition, the size of GO-coated GSPs can be controlled by changing the concentration of gold nano-particles (GNPs) in the oil phase. Moreover, the self-assembly of GNPs endowed the GSP-based nanomaterials with near-infrared absorption and enhanced photothermal conversion properties due to the strong plasmonic coupling effect. Excitingly, after the reduction of the GO shell, the obtained rGO can further improve the photothermal effect, which is useful in photothermal-based theranostic applications. Taking advantage of the dual-enhanced photothermal conversion properties, high photostability and excellent biocompatibility, PEGylated rGO-GSPs could be used as a promising theranostic agent to achieve sensitive photoacoustic detection and efficient photothermal ablation of tumours *in vivo*. We expect that this work, which not only presents a facile approach to construct colloidal superparticles–graphene hybrid nanostructures but also exploits the synergistic effect of the graphene–plasmonic system to achieve a dual-enhanced photothermal effect, will stimulate the development of a novel hybrid nanoplatform with improved properties for biomedical applications.

Supplementary Material

Refer to Web version on PubMed Central for supplementary material.

Acknowledgments

This work was supported by the National Basic Research Program of China (no. 2010CB732403, 2014CB744503), the National Natural Science Foundation of China (no. 21125524, 21475026), and the Intramural Research Program (IRP) of the NIBIB, NIH.

Notes and references

1. Lim EK, Kim T, Paik S, Haam S, Huh YM, Lee K. Chem Rev. 2015; 115:327. [PubMed: 25423180]
2. Lee DE, Koo H, Sun IC, Ryu JH, Kim K, Kwon IC. Chem Soc Rev. 2012; 41:2656. [PubMed: 22189429]
3. Lee JE, Lee N, Kim T, Kim J, Hyeon T. Acc Chem Res. 2011; 44:893. [PubMed: 21848274]
4. Hu SH, Gao X. J Am Chem Soc. 2010; 132:7234. [PubMed: 20459132]
5. Li J, Jiang F, Yang B, Song XR, Liu Y, Yang HH, Cao DR, Shi WR, Chen GN. Sci Rep. 2013; 3:1998. [PubMed: 23770650]
6. Yang Y, Liu F, Liu X, Xing B. Nanoscale. 2013; 5:231. [PubMed: 23154830]
7. Yang K, Hu L, Ma X, Ye S, Cheng L, Shi X, Li C, Li Y, Liu Z. Adv Mater. 2012; 24:1868. [PubMed: 22378564]
8. Lin LS, Cong ZX, Li J, Ke KM, Guo SS, Yang HH, Chen GN. J Mater Chem B. 2014; 2:1031.
9. Lovell JF, Jin CS, Huynh E, Jin H, Kim C, Rubinstein JL, Chan WCW, Cao W, Wang LV, Zheng G. Nat Mater. 2011; 10:324. [PubMed: 21423187]
10. Shanmugam V, Selvakumar S, Yeh CS. Chem Soc Rev. 2014; 43:6254. [PubMed: 24811160]

11. Huynh E, Leung BYC, Helfield BL, Shakiba M, Gandier JA, Jin CS, Master ER, Wilson BC, Goertz DE, Zheng G. *Nat Nanotechnol.* 2015; 10:325. [PubMed: 25822929]
12. Ke K, Lin L, Liang H, Chen X, Han C, Li J, Yang HH. *Chem Commun.* 2015; 51:6800.
13. Lin LS, Cong ZX, Cao JB, Ke KM, Peng QL, Gao J, Yang HH, Liu G, Chen X. *ACS Nano.* 2014; 8:3876. [PubMed: 24654734]
14. Song XR, Wang X, Yu SX, Cao J, Li SH, Li J, Liu G, Yang HH, Chen X. *Adv Mater.* 2015; 27:3285. [PubMed: 25885638]
15. Wang S, Li X, Chen Y, Cai X, Yao H, Gao W, Zheng Y, An X, Shi J, Chen H. *Adv Mater.* 2015; 27:2775. [PubMed: 25821185]
16. Su Y, Wei X, Peng F, Zhong Y, Lu Y, Su S, Xu T, Lee ST, He Y. *Nano Lett.* 2012; 12:1845. [PubMed: 22401822]
17. Ding X, Liow CH, Zhang M, Huang R, Li C, Shen H, Liu M, Zou Y, Gao N, Zhang Z, Li Y, Wang Q, Li S, Jiang J. *J Am Chem Soc.* 2014; 136:15684. [PubMed: 25340966]
18. Dong W, Li Y, Niu D, Ma Z, Gu J, Chen Y, Zhao W, Liu X, Liu C, Shi J. *Adv Mater.* 2011; 23:5392. [PubMed: 21997882]
19. Huang X, El-Sayed IH, Qian W, El-Sayed MA. *J Am Chem Soc.* 2006; 128:2115. [PubMed: 16464114]
20. Huang X, Tang S, Liu B, Ren B, Zheng N. *Adv Mater.* 2011; 23:3420. [PubMed: 21688329]
21. Bhana S, Rai BK, Mishra SR, Wang Y, Huang X. *Nanoscale.* 2012; 4:4939. [PubMed: 22806589]
22. Huang X, Neretina S, El-Sayed MA. *Adv Mater.* 2009; 21:4880. [PubMed: 25378252]
23. Wang X, Wu B, Chen G, Zhao Y, Liu P, Dai Y, Zheng N. *Nanoscale.* 2014; 6:6798. [PubMed: 24827462]
24. Huang X, Tang S, Mu X, Dai Y, Chen G, Zhou Z, Ruan F, Yang Z, Zheng N. *Nat Nanotechnol.* 2011; 6:28. [PubMed: 21131956]
25. Lin J, Wang S, Huang P, Wang Z, Chen S, Niu G, Li W, He J, Cui D, Lu G, Chen X, Nie Z. *ACS Nano.* 2013; 7:5320. [PubMed: 23721576]
26. Huang P, Lin J, Li W, Rong P, Wang Z, Wang S, Wang X, Sun X, Aronova M, Niu G, Leapman RD, Nie Z, Chen X. *Angew Chem, Int Ed.* 2013; 52:13958.
27. Liu Y, Cheng R, Liao L, Zhou H, Bai J, Liu G, Liu L, Huang Y, Duan X. *Nat Commun.* 2011; 2:579. [PubMed: 22146398]
28. Echtermeyer TJ, Britnell L, Jasnok PK, Lombardo A, Gorbachev RV, Grigorenko AN, Geim AK, Ferrari AC, Novoselov KS. *Nat Commun.* 2011; 2:458. [PubMed: 21878912]
29. Paria D, Roy K, Singh HJ, Kumar S, Raghavan S, Ghosh A, Ghosh A. *Adv Mater.* 2015; 27:1751. [PubMed: 25648396]
30. Lim DK, Barhoumi A, Wylie RG, Reznor G, Langer RS, Kohane DS. *Nano Lett.* 2013; 13:4075. [PubMed: 23899267]
31. Moon H, Kumar D, Kim H, Sim C, Chang JH, Kim JM, Kim H, Lim DK. *ACS Nano.* 2015; 9:2711. [PubMed: 25751167]
32. Zedan AF, Moussa S, Turner J, Atkinson G, El-Shall MS. *ACS Nano.* 2013; 7:627. [PubMed: 23194145]
33. Wang P, Liang O, Zhang W, Schroeder T, Xie YH. *Adv Mater.* 2013; 25:4918. [PubMed: 23922275]
34. Bai F, Wang D, Huo Z, Chen W, Liu L, Liang X, Chen C, Wang X, Peng Q, Li Y. *Angew Chem, Int Ed.* 2007; 46:6650.
35. Guardia P, Korobchevskaya K, Casu A, Genovese A, Manna L, Comin A. *ACS Nano.* 2013; 7:1045. [PubMed: 23293834]
36. Hummers WS, Offeman RE. *J Am Chem Soc.* 1958; 80:1339.
37. Nikoobakht B, El-Sayed MA. *Chem Mater.* 2003; 15:1957.
38. Davis ME, Chen ZG, Shin DM. *Nat Rev Drug Discovery.* 2008; 7:771. [PubMed: 18758474]
39. Habash RWY, Bansal R, Krewski D, Alhafid HT. *Crit Rev Biomed Eng.* 2006; 34:459. [PubMed: 17725479]
40. Wang LV, Hu S. *Science.* 2012; 335:1458. [PubMed: 22442475]

41. Kim C, Favazza C, Wang LV. Chem Rev. 2010; 110:2756. [PubMed: 20210338]

Author Manuscript

Author Manuscript

Author Manuscript

Author Manuscript

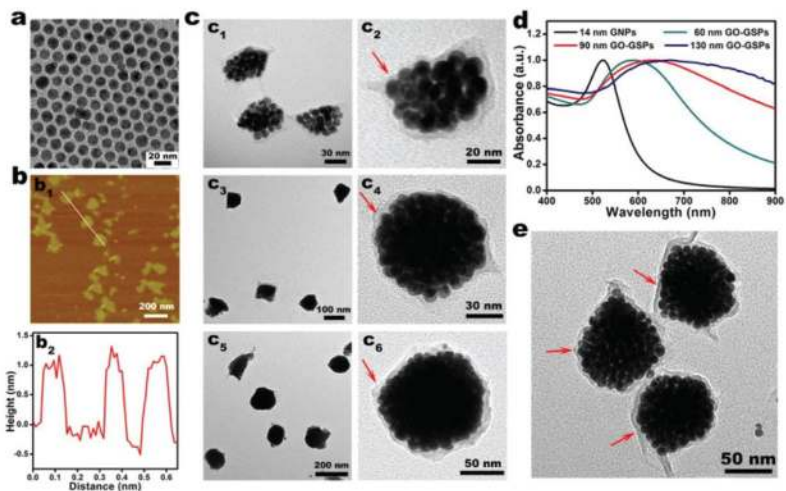


Fig. 1.

(a) TEM image of oleylamine/oleic acid-capped GNPs. (b) Atomic force microscopy (AFM) image (b₁) and the corresponding height image of GO (b₂). (c) TEM images of 60 nm (c₁, c₂), 90 nm (c₃, c₄), and 130 nm (c₅, c₆) GO-GSPs at low (c₁, c₃, c₅) and high (c₂, c₄, c₆) magnifications. The red arrows point to the GO shell. (d) UV-vis spectra of hydrophobic GNPs in chloroform and differently sized GO-GSPs in water. (e) TEM image of 90 nm rGO-GSPs. The red arrows point to the rGO shell.

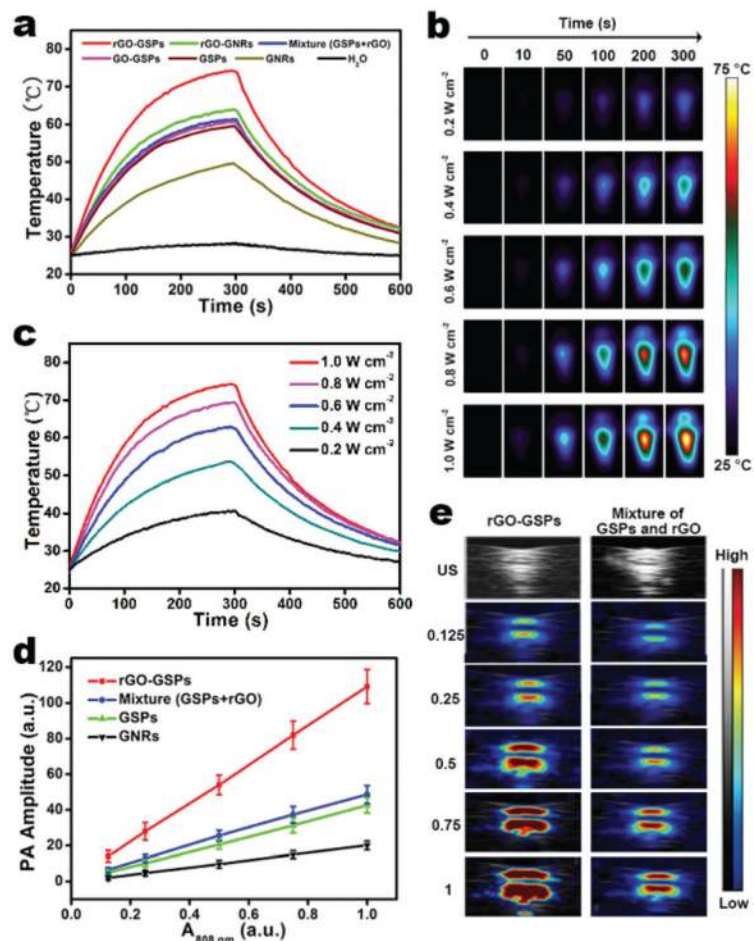


Fig. 2. (a) Temperature elevation of aqueous dispersions of different gold-based nanomaterials ($OD_{808} = 1.0$) exposed to an 808 nm laser (1 W cm^{-2}) as a function of irradiation time. The samples were irradiated for 5 min, and then the laser was turned off. (b) Infrared thermal images and (c) corresponding photothermal heating curves of the aqueous rGO-GSP solution ($OD_{808} = 1.0$) under 808 nm laser irradiation at different power densities. (d) PA signals of rGO-GSPs, mixture of GSPs and rGO, GSPs, and GNRs as a function of OD_{808} . (e) PA images of rGO-GSPs and the mixture of GSPs and rGO at different OD_{808} values.

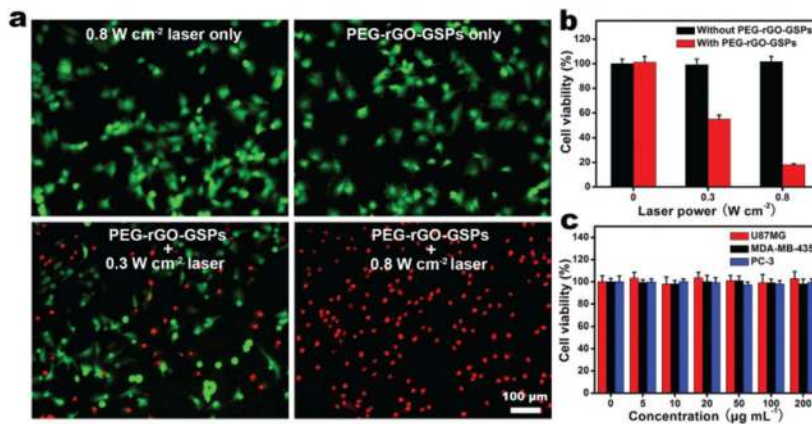


Fig. 3. (a) Fluorescence images of calcein AM (green, live cells) and PI (red, dead cells) co-stained U87MG cells after 4 h of incubation with 100 µg mL⁻¹ PEG-rGO-GSPs and 5 min of exposure to an 808 nm laser at different power densities. (b) Cell viability of U87MG cells treated with 100 µg mL⁻¹ PEG-rGO-GSPs and laser irradiation at different power densities. (c) Cell viability of U87MG, MDA-MB-435, and PC-3 cells after incubation with increased concentrations of PEG-rGO-GSPs for 24 h.

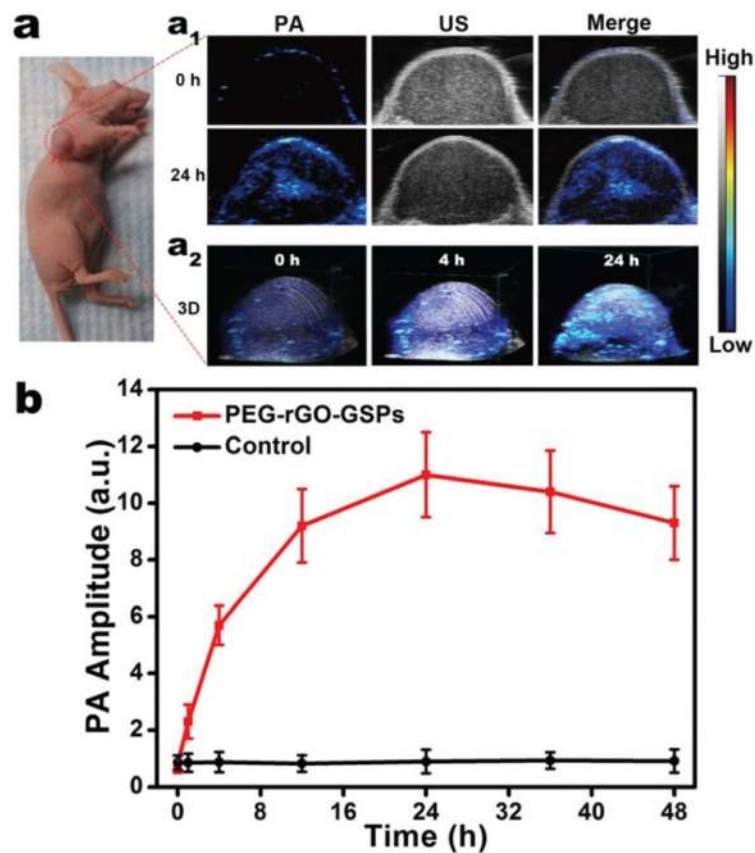


Fig. 4. (a) *In vivo* PA images: (a₁) 2D ultrasonic (US) and PA images of tumour at pre-injection and 24 h post-injection of PEG-rGO-GSPs, and (a₂) 3D images of tumour at 0, 4 or 24 h post-injection of PEG-rGO-GSPs. (b) PA intensities of tumour tissue at different time points after intravenous injection of PEG-rGO-GSPs or PBS as control.

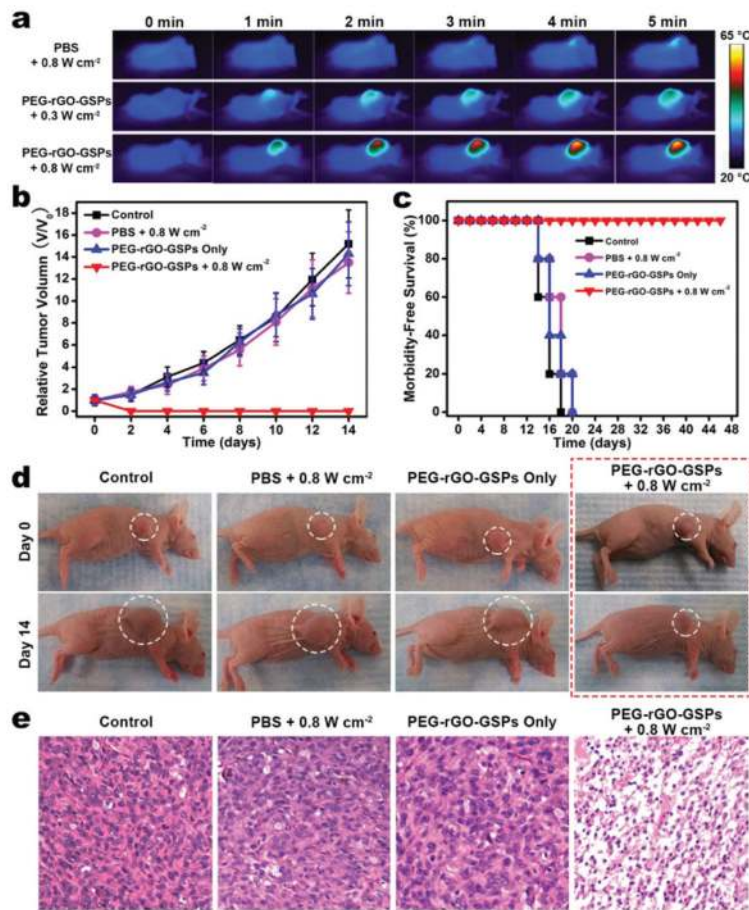
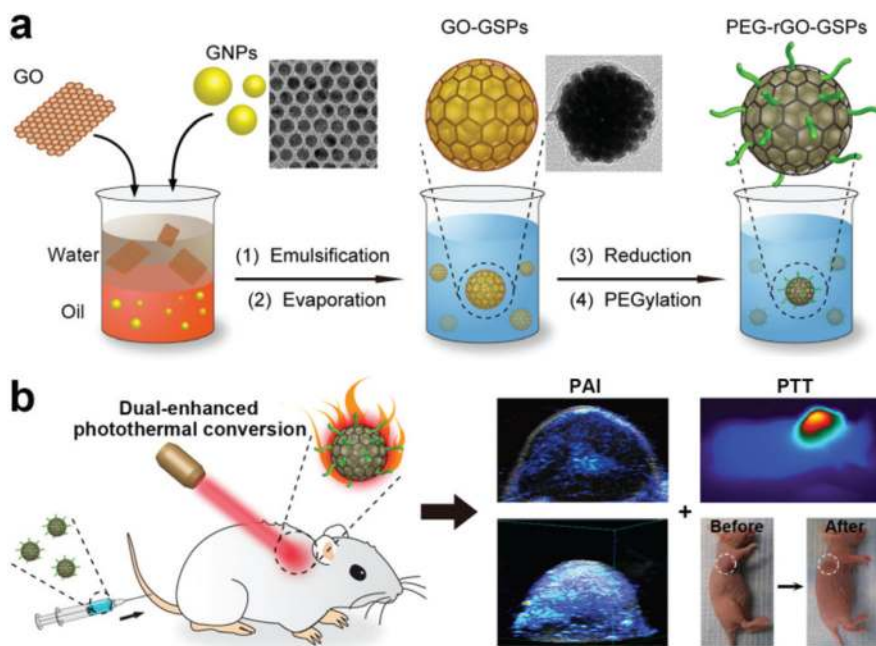


Fig. 5. *In vivo* PTT. (a) Infrared thermal images of U87MG tumour-bearing mice exposed to an 808 nm laser for 5 min at 24 h post-injection of PBS or PEG-rGO-GSPs. (b) Tumour growth curves, (c) survival curves, and (d) representative photos of different groups of mice after various treatments. (e) Images of H&E-stained tumour sections collected from different groups of mice immediately after laser irradiation.

**Scheme 1.**

(a) Schematic illustration of the formation of PEG-rGO-GSPs through an emulsion-based self-assembly method that exploits GO as the emulsifying agent and the precursor of rGO. (b) NIR light-triggered acoustic and thermal theranostics based on PEG-rGO-GSPs with dual-enhanced photothermal conversion properties arising from the plasmonic coupling of adjacent GNPs and the interaction of GSPs with rGO.